Experimental estimation of the local energy balance of the potential-confining electrons in tandem-mirror plasmas

T. Numakura,[a] T. Cho, J. Kohagura, M. Hirata, R. Minami, Y. Miyata, Y. Tomii, Y. Miyake, S. Kiminami, K. Shimizu, N. Morimoto, M. Itou, T. Imai, and S. Miyoshi
Plasma Research Centre, University of Tsukuba, Ibaraki 305-8577, Japan

K. Ogura
Graduate School of Science and Technology, Niigata University, Niigata 950-2181, Japan

(Received 6 May 2006; presented on 10 May 2006; accepted 28 May 2006; published online 21 September 2006)

Our proposed "matrix-type" semiconductor detectors are applied for studying the local energy balance of bulk electrons in the tandem-mirror GAMMA 10. The matrix-type detector array consists of compactly produced six "rows" having different thicknesses of thin dead layers (SiO_2) on its surface. Each row has seven channel units ("columns") for measuring radiation profiles in the radial direction of plasmas. These various SiO_2 layers are, thus, employed as "unbreakable ultrathin radiation-absorption filters" having various thicknesses to distinguish x rays from charge-exchange neutral particles and analyze the radial profiles of both plasma ion and electron temperatures simultaneously. The radial profiles of the energy confinement time and the thermal diffusivity obtained from the local energy balance analysis imply that the improvement of the plasma confinement is associated with the *strong* shear of radial electric fields due to a high plasma confining potentials. © *2006 American Institute of Physics.* [DOI: 10.1063/1.2219404]

I. INTRODUCTION

One of the representative operational modes in GAMMA 10 (Refs. 1–4) is characterized in terms of a hot-ion mode by the use of ion-cyclotron heatings (ICHs).[5] In recent fundamental hot-ion mode experiments, it is reported that by the use of 0.5 kW level gyrotrons[6] in the plug region, four-time progress in the formation of the ion-confining potential ϕ_c, including a record of 3 kV, has been achieved in a hot-ion mode having bulk-ion temperature $T_i = 1-10$ keV. In the above-described mode, *L*-mode like turbulent structures[4,7] are observed in the case without the plug gyrotron injections; in this case, radially produced weak shear of electric fields dE_r/dr and appreciable transverse losses are observed. However, during the application of electron-cyclotron heatings (ECHs) in the plug region, the associated potential rise produces a stronger shear in the central cell (dE_r/dr = several 10 kV/m^2) resulting in the disappearance of such intermittent turbulent vortices with plasma confinement improvement.[4,7]

In the present article, in order to investigate the effect of the radially sheared electric fields on the electron energy confinement, simultaneous observations of detailed information on temperatures of ions and electrons (T_e) in the central-cell region of the GAMMA 10 tandem mirror is made by the use of a single plasma shot alone on the basis of the combination of the theoretical development of radiation analyses[8] and our proposed "matrix-type" semiconductor detector[9] (see Sec. II).

The radial profiles of the electron energy confinement time and the electron thermal diffusivity are derived from the local power-balance analysis by the use of these spatially resolved data on T_e and T_i. During the ECH injections and the formation of the strong sheared electric fields in the central cell, the theoretical results from the electron energy balance analysis with the generalized Pastukhov theory[10] are in good agreement with the experimental data and significant suppression of electron transverse transports is indeed identified (see Sec. III).

II. EXPERIMENTAL APPARATUS

A. GAMMA 10 tandem mirror

GAMMA 10 is a minimum-*B* anchored tandem mirror.[1–4] It has an axial length of 27 m, and the total volume of the vacuum vessel is 150 m^3. The central cell has a length of 6 m and a circularly shaped limiter with a diameter of 36 cm. The magnetic-field intensity at the midplane of the central cell is 0.405 T with a mirror ratio of 5.2. ICHs (Ref. 5) (200 kW at 4.47 or 6.36 MHz, as well as 100 kW at 9.9 or 10.3 MHz) are employed for the central-cell hot-ion production and the anchor stabilization, respectively, after the plasma initiation with both ended magnetoplasma-dynamic (MPD) guns. Two sets of two ECH systems[6] (500 kW at 28 GHz and 1 MW under construction) in the plug and barrier regions are prepared for producing ion-confining and thermal-barrier (ϕ_b) potentials,[1–4] respectively. Potential confined electrons are, in turn, heated due to slowing down powers from the ICH produced hot ions. For the central-cell electrons, no direct wave heatings are applied, and their short collision time of the order of microseconds makes T_e uniform in the axial z direction of the central-cell region.[11] A large part of the database obtained from the GAMMA 10 operations has intensively been investigated and summarized

[a]Electronic mail: numakura@prc.tsukuba.ac.jp

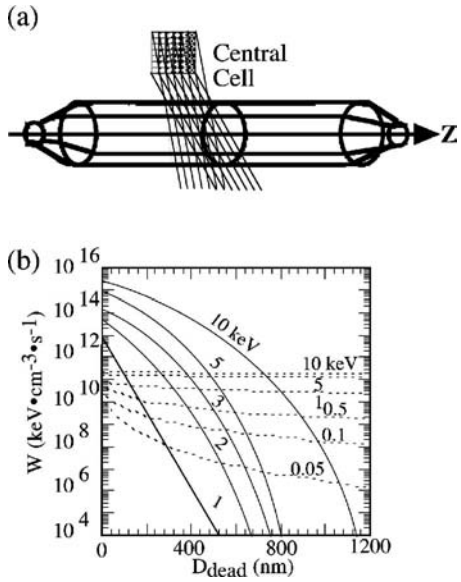

FIG. 1. (a) Schematic drawings of magnetic-flux tube in the central-cell region of the GAMMA 10 tandem mirror along with a matrix-type semiconductor detector and their viewing lines of sight. (b) The solid curves plot the estimated outputs (W) from particle incidence into semiconductor detectors as a function of a SiO_2 dead layer thickness D_{dead}. The dashed curves plot semiconductor x-ray outputs (W).

by using a proposal[1–4] of combining the two major theories, i.e., Cohen's strong electron-cyclotron heating (ECH) theory[12] and the generalized Pastukhov potential-confinement theory.[10]

Figure 1(a) shows schematic drawings of the magnetic-flux tube in the central-cell region of GAMMA 10. Schematic drawings of detector locations and viewing lines of sight of the matrix-type semiconductor detector are illustrated.

B. Matrix-type semiconductor detectors

The matrix-type semiconductor detector[9,11] is fabricated on a 300-μm-thick n-type silicon wafer. The active area of each channel is 0.5×0.5 cm^2. Each detector unit is essentially a p-n junction photodiode having its own output wires. The detector is covered with a 50-nm-thick and a 160-nm-thick aluminum layers for cutting out visible light. The detector is characterized by the formation of six rows with different thicknesses of thin dead layers (SiO_2) with 1, 15, 110, 242, and 495 nm on its surface compactly.

The values of the depletion-layer thickness d_{dep} are designed in the range of 16–21 μm for the present plasma experiments.

A tomographically reconstructed data set in various radiation energy ranges is simultaneously obtained from each detector row having a different ultrathin "SiO_2 radiation absorber" (for more detail, see Refs. 8 and 9). Consequently temporal evolution of energy-resolved perpendicular ion temperatures with regard to the magnetic force lines, T_i and T_e profiles are conveniently attained.

In Fig. 1(b), the solid curves plot the calculated outputs W due to particle incidence. Here, these curves are calculated as a function of the dead-layer thickness D_{dead} and labeled with various values of T_i on the basis of the idea of the use of various thicknesses of a "dead-layer filter" for particle-energy analyses (for more detail, see Ref. 8). A standard table[13] for conversion rates from plasma ions to charge-exchange neutral particles in plasmas is employed for the calculations. The populations of hydrogen atoms n_0 and ions n_i are, for instance, assumed to be 1×10^{14} and 5×10^{18} m^{-3}, respectively, in plasmas.[1–4] As a characteristic feature in Fig. 1(b), one can find the convex curvature ($d^2W/dD_{dead}{}^2<0$) as well as sufficient discrepancy for each curve.

On the other hand, the dashed curves labeled with T_e in Fig. 1(b) plot the calculated outputs W due to x-ray incidence into the same semiconductor detector. Our recently proposed formula[14,15] for semiconductor-detector outputs due to x-ray emission from plasmas is used. One can also find sufficient discrepancy for each dashed curve. A remarkable difference in the curvature (i.e., a concave shape with $d^2W/dD_{dead}{}^2>0$) is found in contrast to that for each solid curve in Fig. 1(b). Such a difference in the shapes of the solid and dashed curves is of use to identify incident species. Therefore, Fig. 1(b) shows the availability of the observations of T_i and T_e for semiconductor detectors having such thin and thick dead-layer filters, respectively.

III. PLASMA EXPERIMENTAL RESULTS AND DISCUSSION

A. Simultaneous T_i and T_e diagnostics

The radial profiles of line-integrated radiation intensities (brightness) in the central cell are obtained during a single plasma discharge by the use of radiation signals in six different energy ranges from the six different detector rows of the matrix detector. The x-ray signals are analyzed to obtain T_e profiles on the basis of the above-described absorption method by fabricating different thicknesses of unbreakable ultrathin dead-layer filters in combination with a 0.72-μm-thick polymer ($-C_8H_8-$) filter for wider energy-range x-ray observations. In Figs. 2(a) and 2(b), two typical profiles of T_i and T_e with time are plotted for comparison. The open and filled circles in Figs. 2(a) and 2(b) represent the profiles before and during ECH injection for plasma-confining potential formation, respectively.

Figure 2(c) shows the radial profile of ϕ_c calculated from Cohen's strong ECH theory[12] [i.e., Eq. (1) in Ref. 4 in GAMMA 10] by the use of the experimental data on T_e and ϕ_b obtained from heavy-ion (Au^0) beam probes[16] during the ECH application period. The theoretical values are in good agreement with the experimental data obtained from ion-energy-spectrometer arrays[17] placed on the end wall of GAMMA 10. The strong sheared electric field in the central cell due to the above-described ϕ_c production clears up the turbulence and drift waves in hot-ion mode plasmas together with plasma-confinement improvement.[4,7,17]

B. The determination of the electron energy confinement time and the electron thermal diffusivity

For the bulk electrons in the central cell, the steady state energy balance equation[3,18] is described as

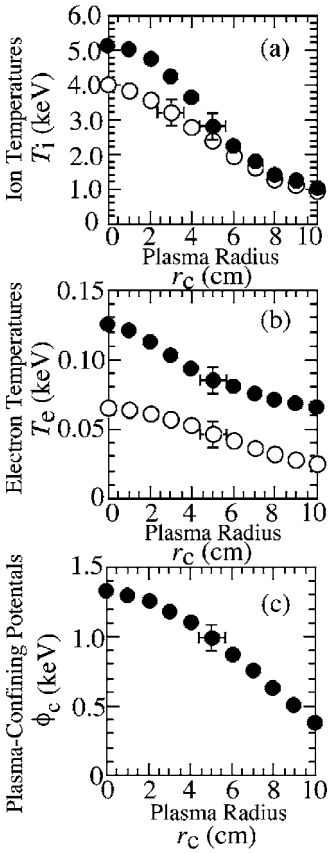

FIG. 2. Radial profiles of T_i and T_e in the central-cell region are plotted in (a) and (b), respectively. The open and filled circles stand for the data before and during ECH injection, respectively. The filled circles in (c) represent ϕ_c calculated from Cohen's strong ECH theory by the use of the experimental data on T_e and ϕ_b obtained from heavy-ion (Au^0) beam probes during the ECH application period. The calculated values are in good agreement with the experimental data obtained from ion-energy-spectrometer arrays placed on the end wall of GAMMA 10.

$$Q_{\text{ion}} = 1.5 n_e T_e / \tau_{\text{pb}}, \tag{1}$$

where Q_{ion} is the ion-electron energy transfer term due to the Coulomb-drag processes and n_e is the electron density obtained from the standard microwave interferometer arrays and τ_{pb} designates the electron energy confinement time estimated by the use of the above-described power balance equation in the steady state with experimental data. In Fig. 3(a), the radial profiles of the ratio of τ_{pb} to τ_{pas}, the electron confinement time calculated from the generalized Pastukhov theory[10] with time, are plotted for comparison. On the other hand, we estimate the radial loss by the use of the difference of Q_{ion} equivalent to the total loss and Pastukhov's predicted axial loss derived from τ_{pas}. In Fig. 3(b), the profiles of the ratio of the thermal diffusivity[19] of the estimated radial loss $\chi_{\perp\text{pb}}$ to the classical thermal diffusivity $\chi_{\perp\text{classic}}$ derived from the Coulomb collision transport theory[20] are plotted. The open and filled circles in Figs. 3(a) and 3(b) represent the profiles before and during ECH injection, respectively. The strong shear of the electric fields E_r (dE_r/dr=several 10 kV/m^2) in the central cell in the region of $r_c < 6$ cm is produced in this plasma shot. The broadband incoherent turbulence and coherent drift waves are suppressed and τ_{pb} and

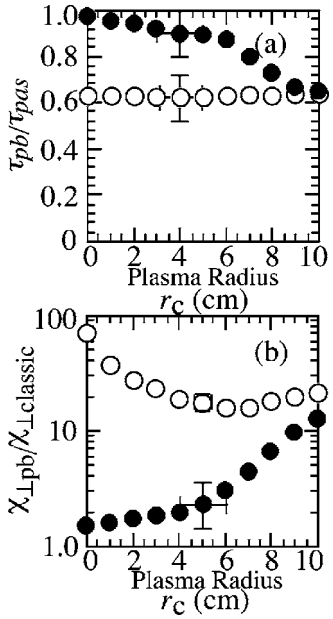

FIG. 3. Radial profiles of the ratio of τ_{pb} to τ_{pas} in (a) and $\chi_{\perp\text{pb}}$ to $\chi_{\perp\text{classic}}$ in (b) are plotted, respectively. The open and filled circles in Fig. 3 represent the profiles before and during ECH injection, respectively. The strong shear of the electric fields E_r (dE_r/dr=several 10 kV/m^2) in the central cell in the region of $r_c < 6$ cm is produced during ECH injection and the weak E_r shear is observed at any r_c before ECH injection. In the strong E_r shear, significant suppression of transverse electron loss is indeed identified.

b $\chi_{\perp\text{pb}}$ are roughly equivalent to τ_{pas} and $\chi_{\perp\text{classic}}$ in the strong shear region, respectively. Before ECH injection, the weak E_r shear and intermitted vortexlike turbulent phenomena and drift waves are observed at any r_c (for more detail, see Ref. 7).

Consequently, the existence of the vortexlike turbulence and drift waves may provide a correlation of the increase of the radial loss with confinement degradation in the case of a weak shear formation, while these turbulence disappear and the radial loss is reduced and confinement is improved with a strong shear formation.

[1] T. Cho *et al.*, Phys. Rev. Lett. **64**, 1373 (1990).
[2] T. Cho *et al.*, Phys. Rev. A **45**, 2532 (1992).
[3] T. Cho *et al.*, Nucl. Fusion **43**, 293 (2003).
[4] T. Cho *et al.*, Nucl. Fusion **45**, 1650 (2005).
[5] M. Ichimura *et al.*, Nucl. Fusion **39**, 1995 (1999).
[6] T. Numakura *et al.*, Fusion Sci. Technol. **47**, 100 (2005).
[7] T. Cho *et al.*, Phys. Rev. Lett. **94**, 085002 (2005).
[8] T. Numakura *et al.*, Plasma Phys. Controlled Fusion **45**, 807 (2003).
[9] T. Numakura *et al.*, Rev. Sci. Instrum. **74**, 2144 (2003).
[10] R. H. Cohen, M. E. Rensink, T. A. Cutler, and A. A. Mirin, Nucl. Fusion **18**, 1229 (1978); R. H. Cohen, *ibid.* **19**, 1295 (1979); **19**, 1693 (1979).
[11] T. Numakura *et al.*, Appl. Phys. Lett. **76**, 146 (2000).
[12] R. H. Cohen, Phys. Fluids **26**, 2774 (1983).
[13] R. L. Freeman and E. M. Jones, Culham Laboratory, UKAEA Research Group Report No. CLM-137, 1974 (unpublished).
[14] J. Kohagura *et al.*, Phys. Rev. E **56**, 5884 (1997).
[15] T. Cho *et al.*, Phys. Rev. A **46**, 3024 (1992).
[16] A. Kojima *et al.*, Rev. Sci. Instrum. **75**, 3652 (2004).
[17] M. Yoshida *et al.*, Rev. Sci. Instrum. **75**, 4344 (2004).
[18] T. Numakura *et al.*, Fusion Sci. Technol. **74**, 222 (2003).
[19] J. Pratt and W. Horton, Phys. Plasmas **13**, 042513 (2006).
[20] P. Helander and D. J. Sigmar, *Collisional Transport in Magnetized Plasmas* (Cambridge University Press, Cambridge, 2002).